EPJ Quantum Technology
a SpringerOpen Journal

RESEARCH   **Open Access**

Quantum image representations based on density matrices in open quantum systems

Yingying Hu[1], Dayong Lu[1*†], Qianqian Zhang[1†] and Meiyu Xu[2†]

*Correspondence:
dayonglu@163.com
[1]School of Mathematics and
Statistics, Henan University, Kaifeng,
475001, China
Full list of author information is
available at the end of the article
†Equal contributors

Abstract

So far, research on quantum image representation has gone through more than 20 years. During this time, the quantum image representation models used have almost all been based on state vectors. However, in practical problems, the environment and the principal quantum system cannot be separated, and isolated quantum systems do not exist in principle. This case is often referred to as an open quantum system. In open quantum systems, many problems involve density matrices, such as the calculation of Von Neumann entropy, the quantization of coherence, and the operator-sum representations of quantum operations. Therefore, the existing quantum image representation models are only suitable for closed quantum systems. To this end, the paper proposes three models that can not only represent quantum images in an open quantum system but also decompose the evolution process of quantum images utilizing operator-sum decomposition. These three models are the representation model of quantum gray-scale images, the tensor product representation model of quantum color images, and the representation model of quantum color images based on mixed states in the Bloch sphere, respectively. All these image representation models have strong correlations among them and are very different from their classical analogues. Between them, the biggest difference is that the paper employs density matrices, inspired by incoherent-coherent states, to represent quantum images rather than classical state vectors. By means of one of the representation models proposed in the paper, we finally demonstrate the evolution process of the quantum image going through the amplitude damping channel.

Keywords: Open quantum systems; Image representations models; Bloch sphere; Quantum noise channels

1 Introduction

In recent decades, the combination of quantum computing [1] and digital image processing [2] has been extensively studied. Quantum image processing (QIP) [3], an area focused on extending conventional image processing tasks and operations to the quantum computing framework, is the new sub-area that has emerged in that regard. The most fundamental problem in this field is the problem of quantum image representation (PQIR) [4–7], the development process of which can be divided into two stages. The first stage starts with the Qubit Lattice representation of quantum images proposed by Benegas-Andraka and Boshi [8] in 2003. This was closely followed by Entangled Image [9] and Real

Springer

Ket [10] representation models. In the second stage, the flexible representation of quantum images (FRQI) [11] was proposed in 2011, followed by the novel enhanced quantum representation of digital images (NEQR) [12] was proposed in 2013, and they are generally considered pioneers of this phase.

However, these representations and applications of quantum images mentioned above are all in closed quantum systems, which require the principal system not to interact with the external environment. In the classical system-environment division, the environmental perturbations to the system can be arbitrarily reduced until their effects are negligible through rational design and division. But the quantum system-environment division is different from that of the classical system-environment, everything that happens in the principal system is always in extensive entanglement with the external environment and even if the energy and matter transfer on the boundary is small enough to be negligible, this entanglement still has a huge impact. Thus, the environment and the principal system can never be separated, and isolated quantum systems cease to exist in principle.

In real physical systems, no matter how weak the coupling that can prevent the principal system from being isolated, the evolution of an open quantum system [13] is eventually plagued by non-unitary features like decoherence and dissipation. The so-called quantum decoherence [14] here is a purely quantum-mechanical effect whereby the system loses its ability to exhibit coherent behavior by getting entangled with the ambient degrees of freedom. Decoherence stands as a serious obstacle common to all applications relying on the capability of maintaining and exploiting quantum coherence. According to the DiVincenzo criteria [15], we require relatively long decoherence times to ensure coherence is preserved during gate operations. Therefore, when the quantum systems we are interested in are no longer isolated or closed but become open quantum systems, it is necessary to quantify the coherence of quantum images in the evolution process. This allows us to better understand and control the effects of these non-unitary features (which can be considered as noise in quantum information processing) on the system's evolution, and take appropriate measures to reduce their negative impact. Hence, it is of significant importance to find better ways to represent quantum images for the future development of quantum image processing.

In the framework of quantum Internet [16], the study of methods and techniques for open-system quantum communication is crucial for building efficient quantum communication networks. Distributed gate models [17] can be used to construct complex and powerful quantum computing networks, where multiple gate model quantum computers can operate and exchange information in a distributed manner. In quantum image transmission, especially under the open system, the effects of noise and distortion need to be considered. At this time the capacity of the quantum noise channel [18] is an important consideration, i.e., the maximum amount of quantum information that can be transmitted in a channel affected by quantum noise. Therefore, when designing and implementing a distributed gate model quantum computing setup, one needs to consider how to ensure the integrity and accuracy of quantum image transmission. The interplay of these aspects promotes the development of the fields of quantum computing and quantum communication, helps to build more reliable quantum communication systems, and promotes the application of quantum technology in various fields.

Inspired by the above problem, the paper considers the PQIR in open quantum systems and gives three specific representation models that can be used to quantify coherence

[19–21] and analyze the dynamic conditions of coherence completely unaffected by noise in open quantum systems. Since the principal system is entangled with the environment in an open quantum system, it is usually described by a mixed state rather than a pure state of the wave function. On this occasion, the following advantages of the state density matrix are demonstrated:

• The density matrix can accurately and completely characterize all measurement properties of open quantum systems.

• Some rigorous frameworks have been proposed to quantify coherence and determine intuitive and computable measures of coherence.

• It can be used to calculate Von Neumann entropy, entropy exchange, and operator-sum representations of quantum operations.

Therefore, the paper utilizes the density matrix to store the gray value of each pixel and completes the preparation process by performing rotation operations on the surface of the Bloch sphere.

The rest of the paper is organized as follows:

–Sect. 2 presents the preliminary knowledge,

–Sect. 3 gives three novel models for representing gray-scale images and RGB color images in open quantum systems and gives the process of quantum image preparation,

–Sect. 4 introduces the environments and quantum noise channels and gives an example of a quantum image coupling with the environment.

Finally, we draw conclusions and outline possible future research tracks.

2 Related work

To date, various quantum image-representation model have been proposed to store and process image information, in quantum computing, such as qubit lattice, entangled image, real ket representation, flexible representation of quantum images (FRQI), novel enhanced quantum representation of digital images (NEQR).

In FRQI, a normalized superposition is used to store used to store position and gray-scale information for all the pixels in an image. The main drawback of this model is that FRQI uses only one qubit to store the gray-scale information of each pixel in the image, which cannot process complex color operations. To improve FRQI, the following proposed NEQR model uses two entangled qubit sequences to store the gray-scale and position information and stores the whole image in the superposition of the two qubit sequences. However, since NEQR can only represent square images of size $2^n \times 2^n$, it cannot be applied to more rectangular images. To solve this problem, NEQR was improved into INEQR [22] to represent quantum images of size $2^{n_1} \times 2^{n_2}$

Furthermore, since in image representation and processing, we usually treat quantum images as two-dimensional data, which are typically represented by floating-point numbers. Therefore, in 2020, Zhang [23] et al. improved the representation of quantum images by increasing the pixel size from positive integers to floating-point representations. This enhancement allows for a finer and more flexible representation of quantum images of arbitrary size, enabling the representation of arbitrary sized 2-D data and accommodating element values of arbitrary precision. Additionally, this method not only handles two-dimensional data of arbitrary size but also facilitates the processing of three-dimensional data through dimensionality reduction. Furthermore, fewer qubits are needed after the dimensionality reduction process compared to the direct preparation of three-dimensional

data. This proposal integrates information about a $H \times W$ 2-D data into a quantum state having it formula in (2.1):

$$|D\rangle = \frac{1}{\sqrt{2}^{h+w}} \left(\sum_{Y=0}^{H-1} \sum_{X=0}^{W-1} |S_{YX}\rangle_F \otimes |YX\rangle \right), \tag{2.1}$$

here, $|YX\rangle$ is the location information, $|S_{YX}\rangle_F$ can store a floating-point number of 2-D data. Therefore, these latest models are also improvements on the FRQI as well as the NEQR. Subsequently, numerous research results in the field of quantum computing have emerged, including the QIC algorithm [24–26], floating point quantum algorithm [27, 28], image scrambling [29], quantum encryption [30], quantum neural networks [31, 32] and, so on.

However, all the above representations are based on closed quantum systems, inspired by [33], when a quantum image transmits quantum information through a noisy channel (i.e., a channel that is not isolated from the environment), assuming that the quantum image is the primary system and undergoes a dynamic evolution process, which can be expressed as the transmission of a quantum image through a noisy quantum channel, the evolution process from initial state to final state is described using density matrices. At the same time, the fact of mathematically describing the evolution of the quantum image in a noisy channel need to use the operators-sum representations of the noisy channel, which inevitably concern the density matrix. Also the use of density matrix description paves the way for the quantization of coherence as well as frozen coherence in future researches.

3 Preliminaries

In this section, we introduce the basic concepts and some knowledge about the Bloch sphere and present the definition of the incoherent-coherent state [34–36].

3.1 Bloch sphere

Comparing the 0 and 1 of classical bits, the two possible states of a single qubit are $|0\rangle$ and $|1\rangle$. In three-dimensional Bloch Sphere, a qubit can be written in the form as:

$$|\psi\rangle = \cos\frac{\theta}{2}|0\rangle + e^{i\phi}\sin\frac{\theta}{2}|1\rangle, \tag{3.1}$$

where $|\cos\frac{\theta}{2}|^2$ and $|e^{i\phi}\sin\frac{\theta}{2}|^2$ respectively represent the probability of becoming $|0\rangle$ and $|1\rangle$, also they satisfy the normalization condition: $|\cos\frac{\theta}{2}|^2 + |e^{i\phi}\sin\frac{\theta}{2}|^2 = 1$. Among them, $0 \le \theta \le \pi$, $0 \le \phi \le 2\pi$, and $e^{i\phi}$ is the relative phase factor. In the Bloch sphere, a point P can be determined by two angles θ and ϕ, i.e., the state vector corresponds to a point on the surface of the Bloch sphere, as it is shown in Fig. 1.

Before we describe the specific use of density matrices in QIP, it is important to introduce the related knowledge of density matrices. To do so, let us first consider the density matrix

Figure 1 Qubit Bloch sphere
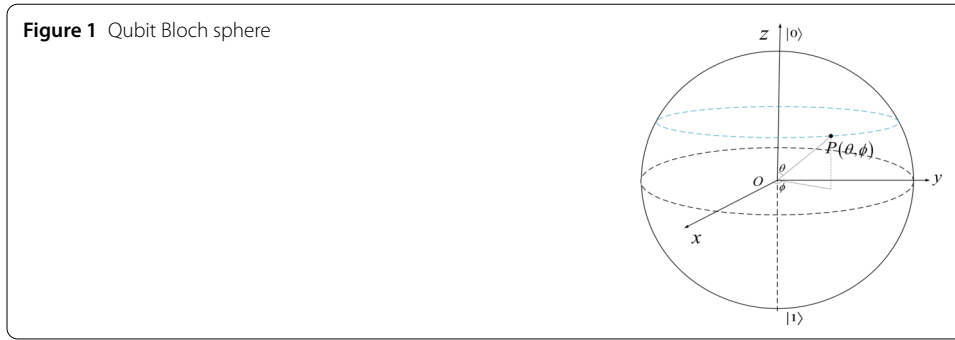
for a single-qubit pure state $|\psi\rangle$ as follows:

$$
\begin{aligned}
\rho(\theta,\phi) &= |\psi\rangle\langle\psi| \\
&= \left(\cos\frac{\theta}{2}|0\rangle + e^{i\phi}\sin\frac{\theta}{2}|1\rangle\right)\left(\cos\frac{\theta}{2}\langle 0| + e^{-i\phi}\sin\frac{\theta}{2}\langle 1|\right) \\
&= \begin{pmatrix} \cos^2\frac{\theta}{2} & e^{-i\phi}\cos\frac{\theta}{2}\sin\frac{\theta}{2} \\ e^{i\phi}\sin\frac{\theta}{2}\cos\frac{\theta}{2} & \sin^2\frac{\theta}{2} \end{pmatrix}.
\end{aligned}
\tag{3.2}
$$

Next, let Bloch vectors $\vec{\upsilon} = (\upsilon_1, \upsilon_2, \upsilon_3)$, where $\upsilon_1 = \sin\theta\cos\phi$, $\upsilon_2 = \sin\theta\sin\phi$, $\upsilon_3 = \cos\theta$, then (3.3) can be rewritten as follows:

$$
\begin{aligned}
\rho(\theta,\phi) &= \frac{1}{2}\left(\begin{bmatrix} 1 & 0 \\ 0 & 1 \end{bmatrix} + \upsilon_1\begin{bmatrix} 0 & 1 \\ 1 & 0 \end{bmatrix} + \upsilon_2\begin{bmatrix} 0 & -i \\ i & 0 \end{bmatrix} + \upsilon_3\begin{bmatrix} 1 & 0 \\ 0 & -1 \end{bmatrix}\right) \\
&= \frac{(I + \vec{\upsilon}\cdot\vec{\sigma})}{2}.
\end{aligned}
\tag{3.3}
$$

Now, since the amplitude of the Bloch vector is unity for a pure state, i.e., $\upsilon_1^2 + \upsilon_2^2 + \upsilon_3^2 = 1$, this is perfectly consistent with the definition of a pure state and we may conclude that the points on the surface of the Bloch sphere depict pure states. Reference [1] also shows that mixed states can be characterized by the condition $\upsilon_1^2 + \upsilon_2^2 + \upsilon_3^2 < 1$, thus the single-qubit mixed states can be represented by the points inside the Bloch sphere.

3.2 Incoherence-coherence state

Quantum coherence represents a basic feature of quantum systems that is not present in the classical world. Coherence is regarded as a precious resource that cannot be generated or increased under a restricted class of operations known as incoherent operations. Unlike other resources, quantum coherence is a basis dependent quantity, a quantum state ρ is said to be incoherent in a given reference basis $\{|i\rangle\}$, if the state is diagonal in this basis, i.e., if $\rho = \sum_i p_i |i\rangle\langle i|$ with some probabilities p_i.

In Chitambar's research assisted coherent distillation task [34], this task arises naturally in bipartite systems where both parties work together to generate the maximal possible coherence on one of the subsystems. For a bipartite system, the reference basis is assumed to be a tensor product of local bases. So in the bipartite system, if a quantum state is called an incoherent-coherent state, then such a state has the following form: $\rho = \sum_i p_i |i\rangle\langle i|^A \otimes \rho_i^B$. Here, ρ_i^B are arbitrary quantum states on quantum subsystem B, and the states $|i\rangle^A$ belong

to the local incoherent basis of quantum subsystem A. Similarly, it is called a coherent-incoherent state if it can be written as $\rho = \sum_i p_i \rho_i^A \otimes |i\rangle\langle i|^B$. Incoherent-coherent and coherent-incoherent states are incoherent in one subsystem.

Despite the fundamental importance of quantum coherence, only very recently have relevant first steps been introduced to a rigorous framework for the quantification of coherence and identified some intuitive and computable measures of coherence [19]. In fact, for the incoherent-coherent state, since one postulate for coherent measurements requires that $C(\rho)$, the coherence of ρ, does not increase on average under selective incoherent operations, then

$$C(\rho) \geq \sum_i p_i C\left(|i\rangle\langle i|^A \otimes \rho_i^B\right) = \sum_i p_i C\left(\rho_i^B\right),$$

for which we choose the incoherent operation for the local projective measurements $\{|i\rangle\langle i|\}$ on the first subsystem. Another postulate for coherent measurements requires that $C(\rho)$ is a convex function of density matrices, which implies

$$C(\rho) \leq \sum_i p_i C\left(|i\rangle\langle i|^A \otimes \rho_i^B\right) = \sum_i p_i C\left(\rho_i^B\right).$$

Therefore, the coherence of incoherent-coherent and coherent-incoherent states is the average of the coherent parts, which proves that the coherence of the incoherent-coherent states can be quantized.
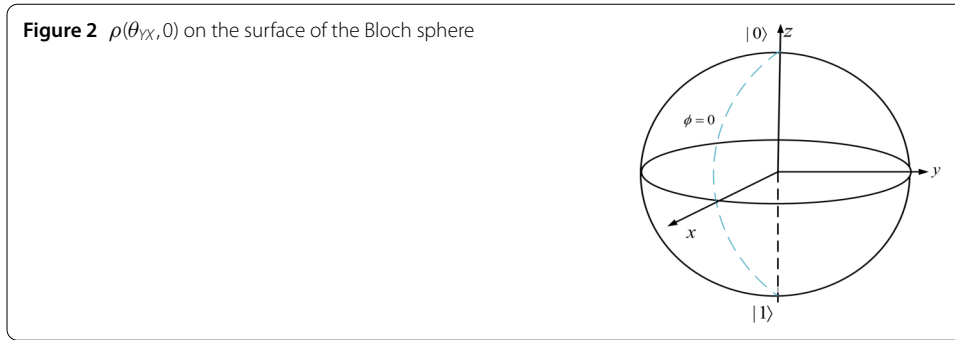
4 Image representation in open quantum systems

All real-world quantum systems always interact with their surroundings to a greater or lesser extent, so that quantum decoherence occurs, such the quantum systems are often called open quantum systems. Representation of quantum images in open quantum systems becomes a crucial step in exploring quantum computers with noise for practical applications. But the quantum image representation models used so far, such as FRQI and NEQR given in (4.1) and (4.2) respectively, are all represented in the form of state vectors as follows:

$$|I_{FRQI}\rangle = \frac{1}{2^n} \sum_{Y=0}^{2^n-1} \sum_{X=0}^{2^n-1} \left(\cos\theta_{YX}|0\rangle + \sin\theta_{YX}|1\rangle\right)|YX\rangle, \tag{4.1}$$

$$\begin{aligned}
|I_{NEQR}\rangle &= \frac{1}{2^n} \sum_{Y=0}^{2^n-1} \sum_{X=0}^{2^n-1} \left|f(Y,X)\right\rangle|YX\rangle \\
&= \frac{1}{2^n} \sum_{Y=0}^{2^n-1} \sum_{X=0}^{2^n-1} \left|C_{YX}^0 C_{YX}^1 \ldots C_{YX}^{q-2} C_{YX}^{q-1}\right\rangle|YX\rangle.
\end{aligned} \tag{4.2}$$

Therefore, the desired density matrices corresponding to (4.1) and (4.2) can be obtained, respectively, by

$$\begin{aligned}
\rho_{FRQI} = \frac{1}{2^{2n}} \sum_{Y=0}^{2^n-1} \sum_{X=0}^{2^n-1} \sum_{Y'=0}^{2^n-1} \sum_{X'=0}^{2^n-1} &\left(\cos\theta_{YX}|0\rangle + \sin\theta_{YX}|1\rangle\right)\left(\cos\theta_{Y'X'}\theta\langle 0| + \sin\theta_{Y'X'}\langle 1|\right) \\
&\otimes |YX\rangle\langle Y'X'|
\end{aligned} \tag{4.3}$$

Figure 2 $\rho(\theta_{YX}, 0)$ on the surface of the Bloch sphere

and

$$\rho_{NEQR} = \frac{1}{2^{2n}} \sum_{Y=0}^{2^n-1} \sum_{X=0}^{2^n-1} \sum_{Y'=0}^{2^n-1} \sum_{X'=0}^{2^n-1} |f(Y,X)\rangle\langle f(Y',X')| \otimes |YX\rangle\langle Y'X'|. \tag{4.4}$$

It is intuitively obvious that both ρ_{FRQI} and ρ_{NEQR} are so complex that their storage and preparation would require a large number of resources, which question demands us to find new tools to represent quantum images in open quantum systems.

4.1 Representation of quantum gray-scale images

In this subsection, combining the encoding method given by FRQI with the incoherent-coherent state, a novel representation for gray-scale images based on density matrices is proposed. Furthermore, the time complexity of the preparation process is also discussed.

The representative expression of a quantum image in the size of $2^n \times 2^n$ can be written as follows:

$$\rho = \frac{1}{2^n} \sum_{Y=0}^{2^n-1} \sum_{X=0}^{2^n-1} |Y\rangle\langle X| \otimes \rho_1(\theta_{YX}),$$

$$\theta_{YX} \in \left[0, \frac{\pi}{2}\right], \quad Y = 0, 1, \ldots, 2^n - 1; X = 0, 1, \ldots, 2^n - 1, \tag{4.5}$$

where $|Y\rangle\langle X|$ encodes the information about position, and $\rho_1(\theta_{YX})$ is a density matrix related to θ_{YX}, which encodes the gray-scale value corresponding to pixel (Y, X) and is specifically expressed as follows:

$$\rho_1(\theta_{YX}) = \left(\cos\theta_{YX}|0\rangle + \sin\theta_{YX}|1\rangle\right)\left(\cos\theta_{YX}\langle 0| + \sin\theta_{YX}\langle 1|\right)$$

$$= \begin{pmatrix} \cos^2\theta_{YX} & \cos\theta_{YX}\sin\theta_{YX} \\ \sin\theta_{YX}\cos\theta_{YX} & \sin^2\theta_{YX} \end{pmatrix}. \tag{4.6}$$

It is obvious that formula (4.4) is equivalent to formula (3.3) with ϕ at 0, i.e., $\rho_1(\theta_{YX}) = \rho(\theta_{YX}, 0)$. This interesting consequence inspires us to represent the intensity in the gray-scale image by employing the quantum states in the Bloch sphere with ϕ at 0. As shown in Fig. 2, $\rho_1(\theta_{YX}) = \rho(\theta_{YX}, 0)$ is the quantum state in the dashed part of the Bloch sphere. Therefore, only the dashed part of the Bloch sphere is used to encode the gray scale.
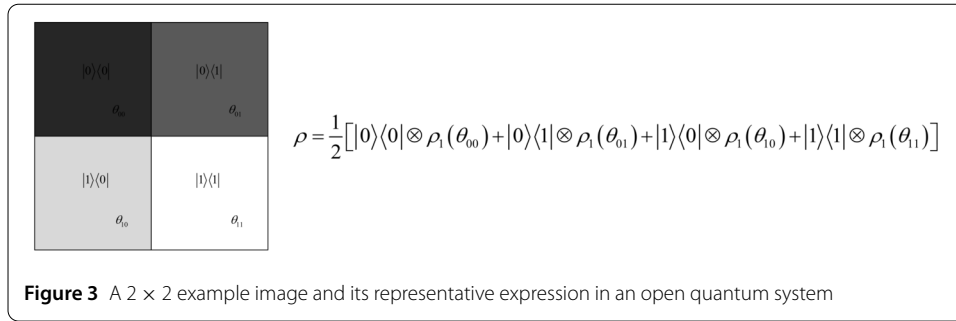
$$\rho = \frac{1}{2}\Big[|0\rangle\langle0|\otimes\rho_1(\theta_{00})+|0\rangle\langle1|\otimes\rho_1(\theta_{01})+|1\rangle\langle0|\otimes\rho_1(\theta_{10})+|1\rangle\langle1|\otimes\rho_1(\theta_{11})\Big]$$

Figure 3 A 2 × 2 example image and its representative expression in an open quantum system

Figure 3 shows a 2×2 quantum image. Compared with the example of FRQI, the obvious difference is that this model utilizes the density matrix to represent the gray scale of pixels instead of the probability amplitude of a single qubit in FRQI.

In quantum computing, computers are usually initialized in well-prepared states. Therefore, the preparation process of transforming the quantum computer from the initialization state to the desired quantum state is necessary. The differences between the evolution of the state vector and that of the density matrix during the preparation process can be specifically described as

$$|\psi\rangle \xrightarrow{U} U|\psi\rangle \quad \text{and} \quad \rho = |\psi\rangle\langle\psi| \xrightarrow{U} U|\psi\rangle\langle\psi|U^\dagger = U\rho U^\dagger. \tag{4.7}$$

There are two ways to prepare the desired quantum states in (4.5). One is based on the relevance of the evolution process between the state vector and the density matrix in (4.7). As a result, in the preparation process, the newly proposed gray-scale image representation, which is encoded based on the density matrix, can replace the state vector in FRQI. Also the same evolutionary operator R_y is adopted in both preparation processes, so it can be concluded that the time complexity of both methods is the same.

The other method is that we take advantage of the fact that the dashed part on the Bloch sphere shown in Fig. 2 represents the intensity of the quantum gray-scale image. So, we can apply the rotation operators to realize the preparation of pixel gray-scale information. Recall that

$$R_x(\theta) = \begin{bmatrix} \cos\frac{\theta}{2} & -i\sin\frac{\theta}{2} \\ -i\sin\frac{\theta}{2} & \cos\frac{\theta}{2} \end{bmatrix}, \qquad R_y(\theta) = \begin{bmatrix} \cos\frac{\theta}{2} & -\sin\frac{\theta}{2} \\ \sin\frac{\theta}{2} & \cos\frac{\theta}{2} \end{bmatrix}, \qquad R_z(\phi) = \begin{bmatrix} 1 & 0 \\ 0 & e^{i\phi} \end{bmatrix}.$$

Any quantum state on the Bloch sphere can be realized by the rotation operators $R_z(\phi)$ and $R_x(\theta)$ acting on the $|0\rangle$, i.e.,

$$R_z\left(\phi + \frac{\pi}{2}\right)R_x(\theta)|0\rangle = \begin{bmatrix} 1 & 0 \\ 0 & e^{i(\phi+\frac{\pi}{2})} \end{bmatrix}\begin{bmatrix} \cos\frac{\theta}{2} & -i\sin\frac{\theta}{2} \\ -i\sin\frac{\theta}{2} & \cos\frac{\theta}{2} \end{bmatrix}\begin{bmatrix} 1 \\ 0 \end{bmatrix}$$
$$= \cos\frac{\theta}{2}|0\rangle + e^{i\phi}\sin\frac{\theta}{2}|1\rangle. \tag{4.8}$$

When discussing the preparation process of gray-scale images in this method, it is worth noting that in equation (4.8), when $\phi = 0$, the effect of $R_z(\phi + \pi/2)R_x(\theta)$ acting on $|0\rangle\langle0|$ is
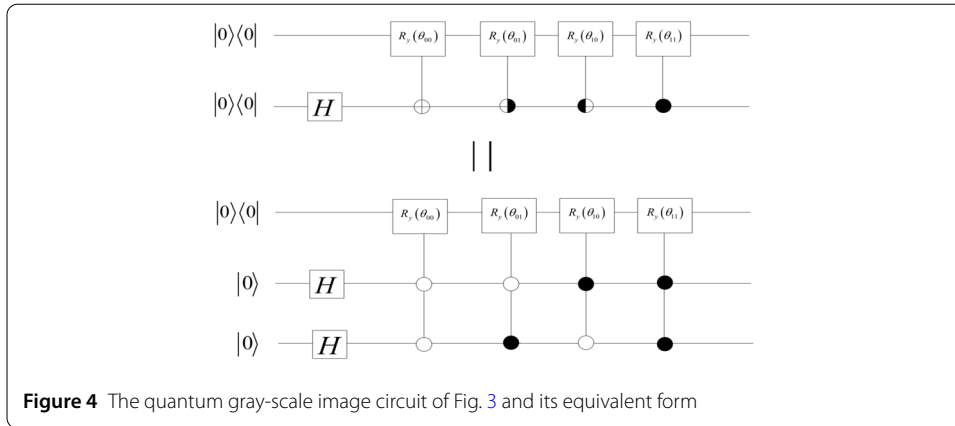
Figure 4 The quantum gray-scale image circuit of Fig. 3 and its equivalent form

equivalent to that of $R_y(\theta)$ acting on $|0\rangle\langle 0|$, i.e.,

$$R_z(\pi/2)R_x(\theta)|0\rangle\langle 0|R_x^\dagger(\theta)R_z^\dagger(\pi/2)$$

$$= \begin{bmatrix} 1 & 0 \\ 0 & i \end{bmatrix} \begin{bmatrix} \cos\frac{\theta}{2} & -i\sin\frac{\theta}{2} \\ -i\sin\frac{\theta}{2} & \cos\frac{\theta}{2} \end{bmatrix} \begin{bmatrix} 1 \\ 0 \end{bmatrix} \begin{bmatrix} 1 & 0 \end{bmatrix} \begin{bmatrix} \cos\frac{\theta}{2} & -i\sin\frac{\theta}{2} \\ -i\sin\frac{\theta}{2} & \cos\frac{\theta}{2} \end{bmatrix} \begin{bmatrix} 1 & 0 \\ 0 & i \end{bmatrix}$$

$$= \begin{pmatrix} \cos^2\theta_{YX} & \cos\theta_{YX}\sin\theta_{YX} \\ \sin\theta_{YX}\cos\theta_{YX} & \sin^2\theta_{YX} \end{pmatrix}$$

$$= R_y(\theta)|0\rangle\langle 0|R_y^\dagger(\theta).$$

Therefore, the quantum gray-scale image circuit of Fig. 3 and its equivalent form can be shown in Fig. 4. In addition, the position information setting in the circuit will be described in detail in Sect. 4.4, Fig. 9.

Recalling the facts that the first preparation method employs the rotation operator $R_y(\theta)$, and the second one utilizes the composite of the rotation operator $R_z(\phi)R_x(\theta)$, it follows from the above equation that the two preparation methods are equivalent, Therefore, the time complexity of the preparation process of (4.5) is similar to that of FRQI.

In contrast, when using the FRQI model or the NEQR model to represent a quantum image in an open quantum system, $4n$ qubits are required to generate the density matrix which stores the position information as far as the position information is concerned, consuming a large amount of resources. However, only $2n$ qubits are needed to store the position information when the density matrix represents the quantum image, saving 50% of qubits. Moreover, as for the computational efficiency, which refers to the complexity of the preparation process, i.e., the number of quantum universal gates, by the way the density matrix shown in Eq. (4.7) evolves, we can learn that the time complexity of the preparation process in Eq. (4.5) is similar to that of FRQI. As for the use of the latest models simply changing the storage of gray values on the basis of FRQI as well as NEQR, the preparation process is similar. Therefore, this approach effectively saves precious qubits and has a unique advantage in dealing with the dynamical evolution of open quantum systems.

4.2 Tensor product representation of quantum color images

The RGB color representation model is one of the most commonly used multi-channel color models, which produces new color information by combining three channels of color information: red, green and blue. Using the RGB color model, a color image can be decomposed into three gray-scale channel images. As mentioned above, the FRQI model has widespread appeal in quantum color images. Inspired by the representation technique in Sect. 4.1, i.e., the gray value at each pixel can be encoded by a pure state $\rho(\theta, \phi)$ with $\phi = 0$ on the surface of the Bloch sphere. A question arose naturally: Whether the encoding technique for gray-scale images can be extended to RGB color images?

The way to deal with this problem is as follows: The gray value information at each pixel is still encoded with $\rho(\theta, \phi)$, but the difference is that ϕ encodes the information of red, green and blue. Specifically speaking, $\rho(\theta, 0)$ encodes color red; $\rho(\theta, \pi/2)$ encodes color green; and $\rho(\theta, \pi)$ encodes color blue. In all these cases, the angle θ is still used to encode the brightness of the color.

The representation of a $2^n \times 2^n$ RGB color image can be written as follows:

$$\rho = \frac{1}{2^n} \sum_{Y=0}^{2^n-1} \sum_{X=0}^{2^n-1} |Y\rangle\langle X| \otimes \rho_2(\overrightarrow{\theta_{YX}}, \overrightarrow{\phi}). \tag{4.9}$$

As can be seen from the above formula, $|Y\rangle\langle X|$ encodes the information about the position and

$$\rho_2(\overrightarrow{\theta_{YX}}, \overrightarrow{\phi}) = \rho(\theta_{YX}^1, 0) \otimes \rho\left(\theta_{YX}^2, \frac{\pi}{2}\right) \otimes \rho(\theta_{YX}^3, \pi),$$

encodes the RGB color information corresponding to the position $|Y\rangle\langle X|$ in quantum images, and at this time $\overrightarrow{\theta_{YX}} = (\theta_{YX}^1, \theta_{YX}^2, \theta_{YX}^3)$, $\theta_{YX}^j \in [0, \pi/2]$, $j = 1, 2, 3$, and $\overrightarrow{\phi} = (0, \pi/2, \pi)$. Among them, $\rho(\theta_{YX}^1, 0)$, $\rho(\theta_{YX}^2, \pi/2)$ and $\rho(\theta_{YX}^3, \pi)$ are used to encode the information of red, green and blue, respectively. According to (3.3), a simple calculation leads to the following conclusion:

$$\rho(\theta_{YX}^1, 0) = \begin{pmatrix} \cos^2 \frac{\theta_{YX}^1}{2} & \cos \frac{\theta_{YX}^1}{2} \sin \frac{\theta_{YX}^1}{2} \\ \sin \frac{\theta_{YX}^1}{2} \cos \frac{\theta_{YX}^1}{2} & \sin^2 \frac{\theta_{YX}^1}{2} \end{pmatrix}, \tag{4.10}$$

$$\rho\left(\theta_{YX}^2, \frac{\pi}{2}\right) = \begin{pmatrix} \cos^2 \frac{\theta_{YX}^2}{2} & -i \cos \frac{\theta_{YX}^2}{2} \sin \frac{\theta_{YX}^2}{2} \\ i \sin \frac{\theta_{YX}^2}{2} \cos \frac{\theta_{YX}^2}{2} & \sin^2 \frac{\theta_{YX}^2}{2} \end{pmatrix}, \tag{4.11}$$

$$\rho(\theta_{YX}^3, \pi) = \begin{pmatrix} \cos^2 \frac{\theta_{YX}^3}{2} & -\cos \frac{\theta_{YX}^3}{2} \sin \frac{\theta_{YX}^3}{2} \\ -\sin \frac{\theta_{YX}^3}{2} \cos \frac{\theta_{YX}^3}{2} & \sin^2 \frac{\theta_{YX}^3}{2} \end{pmatrix}. \tag{4.12}$$

The preparation of gray-scale information can be implemented by applying rotation operators that act on a single qubit on the Bloch sphere according to Sect. 4.1, and the quantum circuits for (4.10), (4.11) and (4.12) are shown in Fig. 5. The method above is a slight modification of that shown in Sect. 4.1. More specifically, we use the three curves on the Bloch sphere to represent the states of the R, G, and B channels, and the preparation process for each curve is the same. When $\phi = 0$, it is observed that the representation is the

Figure 5 The quantum circuits preparing RGB color information
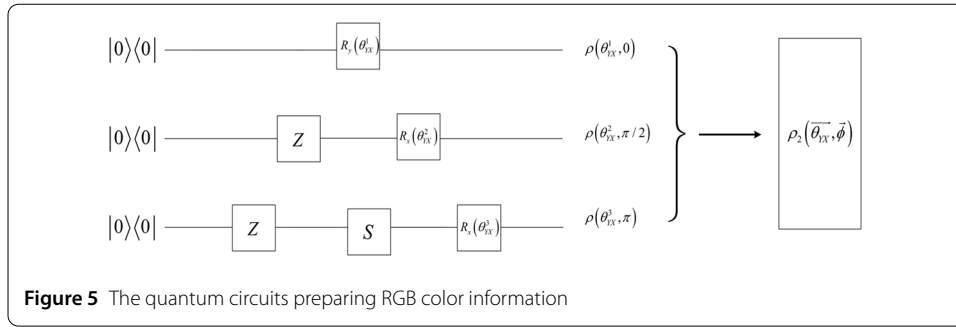
same as that of the gray-scale image. Then, by utilizing equation (4.8), we can further deduce that the effects of $R_z(\phi + \pi/2)R_x(\theta)$ acting on $|0\rangle\langle 0|$ are equal to that of $ZR_x(\theta)$ and $ZSR_x(\theta)$ when $\phi = \pi/2$ and $\phi = \pi$, respectively. Additionally, the time complexity analysis of the preparation process for this representation model will be discussed in Sect. 4.4.

4.3 Mixed state representation of quantum color images

This subsection provides another representation of quantum color images in open systems. The color of each pixel in a quantum color image is determined by the three components R, G, and B, and each component has a value range of 0 to 255. First, the R, G, and B components of the quantum color images are normalized, and then υ_1, υ_2 and υ_3 are applied to encode R, G, and B, respectively. The most intuitive purpose of normalizing R, G, and B components is to reduce the dependence of the color represented by the RGB value on the brightness of the image. Therefore, the information about (R, G, B) of the pixel position (Y, X) in an arbitrary quantum image can be written as

$$\upsilon_{YX}^1 = \frac{R}{255\sqrt{3}}, \qquad \upsilon_{YX}^2 = \frac{G}{255\sqrt{3}} \quad \text{and} \quad \upsilon_{YX}^3 = \frac{B}{255\sqrt{3}}. \tag{4.13}$$

Obviously, $\upsilon_{YX}^1, \upsilon_{YX}^2, \upsilon_{YX}^3 \in [0, 1/\sqrt{3}]$ and $(\upsilon_{YX}^1)^2 + (\upsilon_{YX}^2)^2 + (\upsilon_{YX}^3)^2 \leq 1$. Thus, the corresponding (R, G, B) information for the pixel position (Y, X) in a quantum color image can be encoded by $\overrightarrow{\upsilon}_{YX} = (\upsilon_{YX}^1, \upsilon_{YX}^2, \upsilon_{YX}^3)$.

The second representative expression of a quantum color image in the size of $2^n \times 2^n$ can be written as follows:

$$\rho = \frac{1}{2^n} \sum_{Y=0}^{2^n-1} \sum_{X=0}^{2^n-1} |Y\rangle\langle X| \otimes \rho_{YX}. \tag{4.14}$$

The density matrix ρ_{YX} in (4.14) encodes the information of color corresponding to the pixel position $|Y\rangle\langle X|$, where

$$\rho_{YX} = \frac{(I + \overrightarrow{\upsilon}_{YX} \cdot \vec{\sigma})}{2}, \tag{4.15}$$

in which $\overrightarrow{\upsilon}_{YX} = (\upsilon_{YX}^1, \upsilon_{YX}^2, \upsilon_{YX}^3)$, I is the identical matrix, $\vec{\sigma} = (\sigma_1, \sigma_2, \sigma_3)$ and $\sigma_1, \sigma_2, \sigma_3$ are the Pauli matrices, respectively.

It is worth noting that ρ_{YX} is the density matrix of a certain mixed state ensemble, and so the point corresponding to ρ_{YX} will be in the interior or on the surface of the Bloch sphere.

Figure 6 Relationship between point C and points A and B on the Bloch sphere
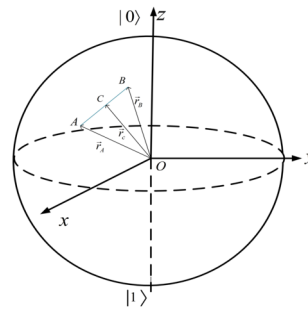
Problem 1 One shortcoming of the model (4.14) is its complexity in preparing the mixed state ρ_{YX}, which limits its practical applicability and confines it to theoretical research. In the paper [37], we learned that, in the general situation, it is possible to purify the mixed state formed by a quantum system Q in interaction with its environment by introducing a reference system R. Specifically, the system R is a dynamically isolated system and has a zero internal Hamiltonian, so that the system R and the quantum system Q can be formed into a joint system RQ to reach a purely entangled state $|\psi^{RQ}\rangle$. Then, the pure state ensemble of quantum system Q can be obtained through the purification process.

And in the paper, the preparation method of the mixed state is explored by utilizing the relation equation between the mixed state and the pure state on the Bloch sphere. Specifically, to realize the preparation of ρ_{YX}, a commonly used approach is employed, where the point corresponding to ρ_{YX} within the Bloch sphere is mapped onto the surface of the Bloch sphere. This mapping allows us to represent ρ_{YX} using a set of pure states. The precise understanding of the relationship between mixed states and pure states is further clarified in Lemma 4.1, which is presented below.

Lemma 4.1 *A mixed state characterized by any point C in the Bloch sphere can be decomposed into two pure states characterized by two points A and B on the Bloch sphere, respectively, where C is on the line connecting A and B.*

Proof From the geometric relationship in Fig. 6, we can have

$$\overrightarrow{r}_C = \overrightarrow{r}_B + \overrightarrow{BC} = \overrightarrow{r}_B + \frac{|CB|}{|AB|}\overrightarrow{BA} = \frac{|CB|}{|AB|}\overrightarrow{r}_A + \left(1 - \frac{|CB|}{|AB|}\right)\overrightarrow{r}_B.$$

Recalling (3.3) we know

$$\rho_A = \frac{1}{2}(I + \overrightarrow{r}_A \cdot \overrightarrow{\sigma}), \qquad \rho_B = \frac{1}{2}(I + \overrightarrow{r_B} \cdot \overrightarrow{\sigma}) \quad \text{and} \quad \rho_C = \frac{1}{2}(I + \overrightarrow{r}_C \cdot \overrightarrow{\sigma}).$$

Let $\lambda = |CB|/|AB|$, then

$$\rho_C = \frac{1}{2}(I + \overrightarrow{r}_C \cdot \overrightarrow{\sigma}) = \frac{1}{2}\{I + [\lambda \overrightarrow{r}_A + (1 - \lambda)\overrightarrow{r}_B] \cdot \overrightarrow{\sigma}\}.$$

In addition,

$$\lambda \rho_A + (1 - \lambda)\rho_B = \frac{1}{2}\left\{ I + \left[\lambda \overrightarrow{r}_A + (1 - \lambda)\overrightarrow{r}_B \right] \cdot \overrightarrow{\sigma} \right\}$$

$$= \frac{1}{2}(I + \overrightarrow{r}_C \cdot \overrightarrow{\sigma}).$$

This finishes the proof.   □

Problem 2 Although Lemma 4.1 gives the answer to Question 1, another question arises naturally, the two pure states, representing the mixed state, corresponding to A and B are obviously not unique, which means that the code based on such pure state decomposition is not uniquely decodable.

Next, the method to solve Problem 2 is given, which is divided into the following two steps.

Step 1: The *RGB* values of the quantum color image are translated into the corresponding points inside the Bloch sphere. For the (R, G, B) information corresponding to the given pixel position (Y, X), the vector $\overrightarrow{v}_{YX} = (v_{YX}^1, v_{YX}^2, v_{YX}^3)$ can be obtained using equation (4.13). Then, it is possible to calculate $(r_{YX}, \theta_{YX}, \phi_{YX})$ for the corresponding points inside the Bloch sphere.

Indeed, assuming that the color information ρ_{YX} at the pixel point (Y, X) has been given in the form of (4.15), for the sake of convenience, we rewrite the vector $\overrightarrow{v}_{YX} \triangleq \overrightarrow{v} = (v_1, v_2, v_3)$ and ignore its position information. According to the spherical coordinate transformation:

$$v_1 = r \sin\theta_0 \cos\phi_0, \qquad v_2 = r \sin\theta_0 \sin\phi_0, \qquad v_3 = r \cos\theta_0 \quad \text{and} \quad r \in [0, 1].$$

A direct calculation gives $B(r, \theta_0, \phi_0)$, where $\theta_0 \in [0, \pi/2], \phi_0 \in [0, \pi/2]$. The location of point B is shown in Fig. 7.
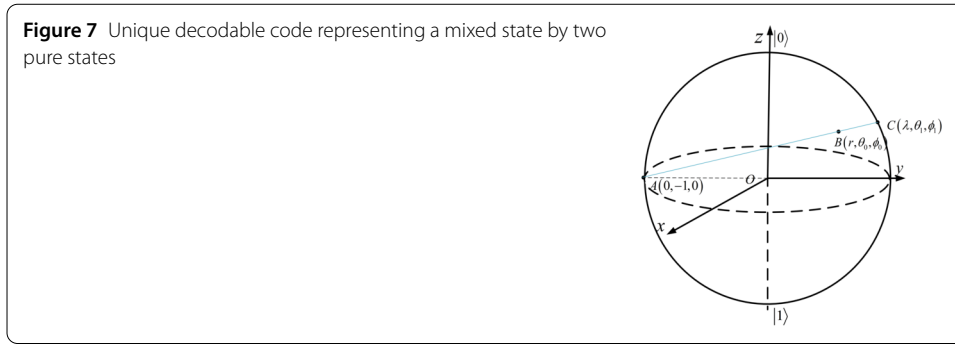
Step 2: At fixed point A, the mixed state $B(v_1, v_2, v_3)$ inside the Bloch sphere can be uniquely decomposed into pure states.

In order to obtain such a result, we first give a fixed point $A(0, -1, 0)$ on the Bloch sphere (see Fig. 7). Then, the half-line $\overrightarrow{AB}$ intersects the surface of the Bloch sphere at the point $C(v_1', v_2', v_3')$, where C is the point related to B that we are looking for. According to the following simultaneous equations to find the intersection, the coordinates of point C, of the half-line $\overrightarrow{AB}$ with the Bloch sphere

$$\begin{cases} x^2 + y^2 + z^2 = 1, \\ \frac{x}{v_1} = \frac{y+1}{v_2+1} = \frac{z}{v_3}, \end{cases}$$

we have

$$v_1' = \frac{2v_1(v_2 + 1)}{v_1^2 + v_3^2 + (v_2 + 1)^2},$$

$$v_2' = \frac{2(v_2 + 1)^2}{v_1^2 + v_3^2 + (v_2 + 1)^2} - 1, \tag{4.16}$$

Figure 7 Unique decodable code representing a mixed state by two pure states

$$v_3' = \frac{2v_3(v_2 + 1)}{v_1^2 + v_3^2 + (v_2 + 1)^2}.$$

Since C is on the surface of the Bloch sphere, through geometric relationships we have

$$\theta_1 = \arccos v_3' = \arccos \frac{2v_3(v_2 + 1)}{v_1^2 + v_3^2 + (v_2 + 1)^2},$$

$$\phi_1 = \arctan \frac{v_2'}{v_1'} = \arctan \frac{(v_2 + 1)^2 - v_1^2 - v_3^2}{2v_1(v_2 + 1)}. \tag{4.17}$$

In order to establish a unique decodable relation between B and C, the parameter λ is also introduced, where $\lambda = |AB|/|AC|$. Here, $|AB|$ and $|AC|$ represent the length of line segments AB and AC respectively. So far, the mixed state B is jointly determined by pure states A, C and the parameter λ. The whole mapping procedure of a unique decodable code representing a mixed state by two pure states can be seen in Fig. 7.

To better understand the encoding method presented above, two examples are given next.

Example 1 Here we assume that if the information of (R, G, B) is $(0, 0, 0)$, it corresponds to the fully mixed state, i.e., $\rho_{YX} = I/2$, and the point is the center of the Bloch sphere. Through simple calculation, we can have $\theta_1 = \pi/2$, $\phi_1 = \pi/2$ and $\lambda = 1/2$.

Example 2 Calculate the coordinates of point C on the surface of the Bloch sphere and the parameter λ, which jointly determine (R, G, B) information as $(255, 0, 0)$.

It is easy to know that the coordinates $B(v_1, v_2, v_3)$ of the mixed state are $(\sqrt{3}/3, 0, 0)$. So we have

$$r \sin\theta \cos\phi = v_1 = \frac{\sqrt{3}}{3}, \qquad r \sin\theta \sin\phi = v_2 = 0 \quad \text{and} \quad r \cos\theta = v_3 = 0.$$

By straightforward calculation, we can get the following results: $r = \sqrt{3}/3$, $\theta = \pi/2$ and $\phi = 0$. Using the fact that $A(0, -1, 0)$ is given, then we have $\overrightarrow{AB} = (\sqrt{3}/3, 1, 0)$ and $|AB| = 2\sqrt{3}/3$.

Combining (4.16) with (4.17), it can be calculated that the intersection point $C(v_1', v_2', v_3')$ of the half-line $\overrightarrow{AB}$ and the surface of the Bloch sphere is $C(\sqrt{3}/2, 1/2, 0)$. Therefore, we know that $|AC| = \sqrt{3}$, $\theta_1 = \pi/2$, $\phi_1 = \pi/6$ and $\lambda = |AB|/|AC| = 2/3$.

By now, the conclusion can be drawn: When (R, G, B) is $(255, 0, 0)$, the mixed state can be uniquely decodable decomposed into the pure state $C(\theta_1, \phi_1)$ and the parameter $\lambda = 2/3$.

Finally, based on the above discussion, an alternative representation in the size of $2^n \times 2^n$ RGB color image is as shown in (4.18):

$$\rho = \frac{1}{2^n} \sum_{Y=0}^{2^n-1} \sum_{X=0}^{2^n-1} |Y\rangle\langle X| \otimes \rho'_{YX} \otimes |\lambda_{YX}\rangle\langle\lambda_{YX}|. \tag{4.18}$$

The new model proposed here is called the mixed state representation of quantum color images, abbreviated as the MSR-QCI model. Supposing that the accuracy of the parameter λ_{YX} is 2^{-q}, i.e., $\lambda_{YX} \in [0, 2^{-q} - 1]$, then the parameter λ_{YX} corresponding to the pixel (Y, X) is encoded as follows:

$$\lambda_{YX} = C_{YX}^{-1} C_{YX}^{-2} \ldots C_{YX}^{-q-1} C_{YX}^{-q}, \qquad C_{YX}^{-k} \in \{0, 1\}, \quad k = 1, 2, \ldots, q.$$

In (4.18), $|Y\rangle\langle X|$ is used to represent position information of pixel, ρ'_{YX} refers to the representation of the mapping of the mixed states within the Bloch sphere to the pure states of the corresponding sphere, while $\rho'_{YX} \otimes |\lambda_{YX}\rangle\langle\lambda_{YX}|$ encodes the color information.

4.4 Preparation process of MSR-QCI model

In order to obtain the desired quantum image on the quantum computer, the preparation process of the MSR-QCI model is necessary and is described in this subsection. From the representation of the MSR-QCI model, $n + q + 1$ qubits are needed to construct the quantum image model for a $2^n \times 2^n$ RGB color image.

The first step is to prepare $n + q + 1$ qubits and to set all of them to $|0\rangle\langle 0|$. The initial state can be expressed by

$$\rho'_0 = \left(|0\rangle\langle 0|\right)^{\otimes(n+q+1)}. \tag{4.19}$$

Recalling the discussion in Sect. 4.3, the desired pure state $C(\theta_1, \phi_1)$ and parameter $|\lambda\rangle$ can be calculated in advance. The preparation process for the MSR-QCI model is now divided into three steps.

Step 1: In this step, single qubit gates I and H are used to prepare position information, which converts the initial state ρ'_0 to the intermediate state ρ'_1, where

$$I = \begin{bmatrix} 1 & 0 \\ 0 & 1 \end{bmatrix}, \qquad H = \frac{1}{\sqrt{2}} \begin{bmatrix} 1 & 1 \\ 1 & -1 \end{bmatrix}.$$

The whole quantum operation in step 1 can be expressed by U_1:

$$U_1 = H^{\otimes n} \otimes I^{\otimes(q+1)}.$$

(4.20) interprets the transformation from the initial state ρ'_0 to the intermediate state ρ'_1. After this step, the position information for all the pixels is stored in the MSR-QCI model.

$$\begin{aligned} U_1\left(\rho'_0\right)U_1^\dagger &= \left(H^{\otimes n} \otimes I^{\otimes(q+1)}\right)\left(|0\rangle\langle 0|\right)^{\otimes(n+q+1)}\left(H^{\otimes n} \otimes I^{\otimes(q+1)}\right)^\dagger \\ &= \frac{1}{2^n} \sum_{Y=0}^{2^n-1} \sum_{X=0}^{2^n-1} |Y\rangle\langle X| \otimes \left(|0\rangle\langle 0|\right)^{\otimes(q+1)} \\ &= \rho'_1. \end{aligned} \tag{4.20}$$

Step 2: To prepare the quantum color image, it remains to set the information of color for every pixel. In effect, this step can also apply the rotation of qubit on the surface of the Bloch sphere to realize the preparation of pixel color information. Given pixel position (Y, X), define the quantum controlled rotation operation U_{YX} as follows:

$$U_{YX} = \left(\sum_{\substack{j=0 \\ (j,i) \neq (Y,X)}}^{2^n-1} \sum_{i=0}^{2^n-1} |j\rangle\langle i| \otimes I^{\otimes(q+1)} \right) + |Y\rangle\langle X| \otimes \Omega_{YX}(\theta_1, \phi_1) \otimes I^{\otimes q},$$

where

$$\Omega_{YX}(\theta_1, \phi_1) = R_z\left(\phi_1 + \frac{\pi}{2} \right) R_x(\theta_1).$$

Acting $\Omega_{YX}(\theta_1, \phi_1)$ on the initial state $|0\rangle\langle 0|$ gives us:

$$\Omega_{YX}(\theta_1, \phi_1)|0\rangle\langle 0|\Omega_{YX}^{\dagger}(\theta_1, \phi_1)$$

$$= R_z\left(\phi_1 + \frac{\pi}{2} \right) R_x(\theta_1)|0\rangle\langle 0|R_x^{\dagger}(\theta_1)R_z^{\dagger}\left(\phi_1 + \frac{\pi}{2} \right)$$

$$= \left(\cos\frac{\theta_1}{2}|0\rangle + e^{i\phi_1}\sin\frac{\theta_1}{2}|1\rangle \right)\left(\cos\frac{\theta_1}{2}\langle 0| + e^{-i\phi_1}\sin\frac{\theta_1}{2}\langle 1| \right)$$

$$= \frac{(I + \overrightarrow{v'}_{YX} \cdot \overrightarrow{\sigma})}{2}$$

$$= \rho'_{YX}.$$

Then U_{YX} acting on ρ'_1 can obtain the following result:

$$U_{YX}\rho'_1 U_{YX}^{\dagger}$$

$$= U_{YX}\left[\frac{1}{2^n} \sum_{j=0}^{2^n-1} \sum_{i=0}^{2^n-1} |j\rangle\langle i| \otimes (|0\rangle\langle 0|)^{q+1} \right] U_{YX}^{\dagger}$$

$$= \frac{1}{2^n}\left[\sum_{\substack{j=0 \\ (j,i) \neq (Y,X)}}^{2^n-1} \sum_{i=0}^{2^n-1} |j\rangle\langle i| \otimes |0\rangle\langle 0| \otimes (|0\rangle\langle 0|)^q \right. \tag{4.21}$$

$$\left. + |Y\rangle\langle X| \otimes \Omega_{YX}|0\rangle\langle 0|\Omega_{YX}^{\dagger} \otimes (|0\rangle\langle 0|)^q \right]$$

$$= \frac{1}{2^n}\left[\sum_{\substack{j=0 \\ (j,i) \neq (Y,X)}}^{2^n-1} \sum_{i=0}^{2^n-1} |j\rangle\langle i| \otimes |0\rangle\langle 0| \otimes (|0\rangle\langle 0|)^q + |Y\rangle\langle X| \otimes \rho'_{YX} \otimes (|0\rangle\langle 0|)^q \right].$$

Therefore, the whole rotation operator U_2 can be defined as

$$U_2 \rho'_1 U_2^{\dagger} = U_{2^n-1}U_{2^n-2}\ldots U_{01}U_{00}\rho'_1 U_{00}^{\dagger}U_{01}^{\dagger}\ldots U_{2^n-2}^{\dagger}U_{2^n-1}^{\dagger}.$$

Through the quantum operator U_2, the intermediate state ρ_1' is transformed into ρ_2'.

$$U_2 \rho_1' U_2^\dagger = \frac{1}{2^n} \sum_{Y=0}^{2^n-1} \sum_{X=0}^{2^n-1} |Y\rangle\langle X| \otimes \rho_{YX}' \otimes (|0\rangle\langle 0|)^q$$

$$= \rho_2'.$$

Step 3: The final step is to prepare the parameter $|\lambda_{YX}\rangle$ at each pixel position (Y, X), which is expressed as a fixed-point decimal with an accuracy of 2^{-q} and is stored in the quantum circuits using q qubits. In effect, we also need to divide the last step into 2^{2n} sub-operations to store the parameter information of each pixel. Fixed pixel position (Y, X), the corresponding quantum sub-operation Λ_{YX} is defined as follows:

$$\Lambda_{YX} = \left(\sum_{\substack{j=0 \\ (j,i)\neq(Y,X)}}^{2^n-1} \sum_{i=0}^{2^n-1} |j\rangle\langle i| \otimes I^{\otimes(q+1)} \right) + |Y\rangle\langle X| \otimes I \otimes \Upsilon_{YX}, \tag{4.22}$$

where Υ_{YX} is a quantum operator as shown in (4.23), which is the value-setting operator for pixel position (Y, X):

$$\Upsilon_{YX} = \bigotimes_{i=1}^{q} \Upsilon_{YX}^i, \qquad \Upsilon_{YX}^i : |0\rangle\langle 0| \to |0 \oplus C_{YX}^{-i}\rangle\langle 0 \oplus C_{YX}^{-i}|, \quad i = 1, 2, \ldots, q. \tag{4.23}$$

From (4.23), if $C_{YX}^{-i} = 1$, Υ_{YX}^i is an n-CNOT gate. Otherwise, it is a quantum identity gate that will do nothing on the quantum state. Therefore, the quantum transformation of Υ_{YX} to set parameter $|\lambda_{YX}\rangle$ for the pixel is as follows:

$$\Upsilon_{YX} (|0\rangle\langle 0|)^{\otimes q} \Upsilon_{YX}^\dagger = \bigotimes_{i=1}^{q} |0 \oplus C_{YX}^{-i}\rangle\langle 0 \oplus C_{YX}^{-i}|$$

$$= \bigotimes_{i=1}^{q} |C_{YX}^{-i}\rangle\langle C_{YX}^{-i}|$$

$$= |\lambda_{YX}\rangle\langle \lambda_{YX}|.$$

Therefore, the intermediate state ρ_2' is transformed as in (4.24):

$$\Lambda_{YX} \rho_2' \Lambda_{YX}^\dagger$$

$$= \Lambda_{YX} \left[\frac{1}{2^n} \sum_{Y=0}^{2^n-1} \sum_{X=0}^{2^n-1} |Y\rangle\langle X| \otimes \rho_{YX}' \otimes (|0\rangle\langle 0|)^q \right] \Lambda_{YX}^\dagger$$

$$= \frac{1}{2^n} \bigotimes_{i=1}^{q} \left[\sum_{\substack{j=0 \\ (j,i)\neq(Y,X)}}^{2^n-1} \sum_{i=0}^{2^n-1} |j\rangle\langle i| \otimes \rho_{ji}' \otimes (|0\rangle\langle 0|)^{\otimes q} \right. \tag{4.24}$$

$$\left. + |Y\rangle\langle X| \otimes \rho_{YX}' \otimes \Upsilon_{YX} (|0\rangle\langle 0|)^{\otimes q} \Upsilon_{YX}^\dagger \right]$$
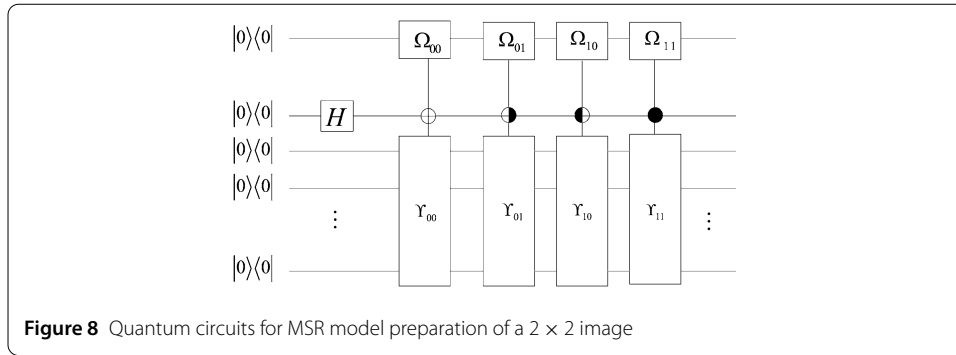
Figure 8 Quantum circuits for MSR model preparation of a 2×2 image

$$= \frac{1}{2^n} \left[\sum_{\substack{j=0 \\ (j,i) \neq (Y,X)}}^{2^n-1} \sum_{i=0}^{2^n-1} |j\rangle\langle i| \otimes \rho'_{ji} \otimes \left(|0\rangle\langle 0|\right)^{\otimes q} + |Y\rangle\langle X| \otimes \rho'_{YX} \otimes \left|\lambda'_{YX}\right\rangle\langle\lambda_{YX}| \right].$$

It can be seen from the above formula that every operator Λ_{YX} only sets the parameter $|\lambda_{YX}\rangle$ of its corresponding pixel position. Therefore, the whole work U_3 of step 3 consisting of all the sub-operators is as follows:

$$U_3 \rho'_2 U_3^\dagger = \Lambda_{2^n-1} \Lambda_{2^n-2} \ldots \Lambda_{01} \Lambda_{00} \rho'_1 \Lambda_{00}^\dagger \Lambda_{01}^\dagger \ldots \Lambda_{2^n-2}^\dagger \Lambda_{2^n-1}^\dagger$$

$$= \frac{1}{2^n} \sum_{Y=0}^{2^n-1} \sum_{X=0}^{2^n-1} |Y\rangle\langle X| \otimes \rho'_{YX} \otimes |\lambda_{YX}\rangle\langle\lambda_{YX}| \tag{4.25}$$

$$= \rho.$$

After the three steps described above, the entire preparation is done.

(4.26) illustrates the representation of a quantum color image of size 2×2 in the MSR model, and Fig. 8 shows the detailed quantum circuits for this 2×2 image MSR model.

$$\rho = \frac{1}{4} \begin{bmatrix} (I + \overrightarrow{\upsilon'}_{00} \cdot \overrightarrow{\sigma}) \otimes |\lambda_{00}\rangle\langle\lambda_{00}| & (I + \overrightarrow{\upsilon'}_{01} \cdot \overrightarrow{\sigma}) \otimes |\lambda_{01}\rangle\langle\lambda_{01}| \\ (I + \overrightarrow{\upsilon'}_{10} \cdot \overrightarrow{\sigma}) \otimes |\lambda_{10}\rangle\langle\lambda_{10}| & (I + \overrightarrow{\upsilon'}_{11} \cdot \overrightarrow{\sigma}) \otimes |\lambda_{11}\rangle\langle\lambda_{11}| \end{bmatrix}. \tag{4.26}$$
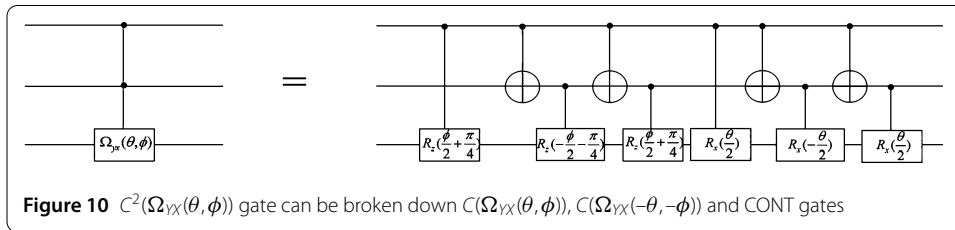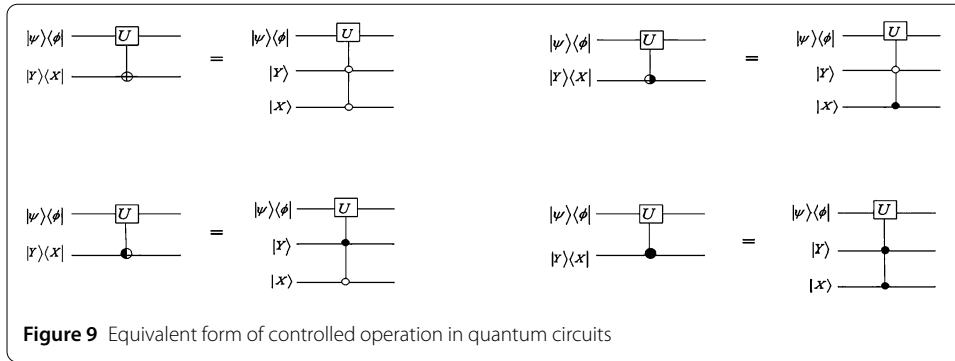
step 1 Preparation of position information:

$$H|0\rangle\langle 0|H^\dagger = \frac{|0\rangle + |1\rangle}{\sqrt{2}} \cdot \frac{\langle 0| + \langle 1|}{\sqrt{2}} = \frac{|0\rangle\langle 0| + |0\rangle\langle 1| + |1\rangle\langle 0| + |1\rangle\langle 1|}{2}.$$

step 2 Use the quantum control rotation operator Ω_{YX} to obtain the intermediate state ρ'_2.

step 3 For convenience, suppose that $\lambda_{00} = \lambda_{01} = \lambda_{10} = \lambda_{11} = (3/4)_{10} = (11000000)_2$. By means of the operators Λ_{YX}, we can finish the preparation process of parameters λ_{YX}.

In quantum computation, computers are usually initialized in well-prepared states. When we discussed the time complexity of quantum image preparation, a complex operation needs to be broken down into simple gates. Thus, the controlled operation in which the control qubit is the position qubit and the target qubit is the color qubit in Fig. 8 has its equivalent form as shown in Fig. 9.

Next, the time complexity of quantum image preparation will be discussed. To begin with, the quantum operation of step 1 is U_1. The transform U_1 can be directly implemented by $2n$ Hadamard gates, and it is known that the time complexity of step 1 is $O(n)$.

Figure 9 Equivalent form of controlled operation in quantum circuits

Figure 10 $C^2(\Omega_{YX}(\theta,\phi))$ gate can be broken down $C(\Omega_{YX}(\theta,\phi))$, $C(\Omega_{YX}(-\theta,-\phi))$ and CONT gates

However, the work of step 2 is more complex than that of step 1. The unitary transform U_2, for a given coordinates (θ,ϕ), can be implemented by 2^{2n} controlled rotations $\Omega_{YX}(\theta,\phi)$ or generalized-$C^{2n}(\Omega_{YX}(\theta,\phi)) = C^{2n}[R_z(\phi + \frac{\pi}{2})R_x(\theta)]$ [1]. Furthermore, $C^{2n}(\Omega_{YX}(\theta,\phi))$ operation can be broken down into $2 \cdot (2^{2n} - 1)$ single-qubit operations, i.e., $R_x(\frac{\theta}{2}), R_x(-\frac{\theta}{2})$ and $R_z(\frac{\phi+\pi/2}{2}), R_z(-\frac{\phi+\pi/2}{2})$, and $2 \cdot (2^{2n} - 2)$ CNOT operations. Therefore, it is concluded that the time complexity of step 2 is $2^{2n} \times 2[(2^{2n-1} - 1) + (2^{2n-1} - 2)]$. And the example when $n = 1$ is shown in Fig. 10.

In addition, it is known that every 2n-CNOT gate can be decomposed into $16(8n - 8)$ 2-CNOT gates (Toffoli gates), and a Toffoli gate can be decomposed into 8 CNOT and 8 single-qubit gates [1]. So the time complexity of step 3 is no more than $16 \times 16 \times 2^{2n} \times q \times (8n - 8)$ with enough ancillary qubits, i.e., $O(qn2^{2n})$.

The total number of single-qubit and double-qubit operations used to prepare the MSR-QCI mode is

$$2n + 2^{2n} \times 2\big[\big(2^{2n-1} - 1\big) + \big(2^{2n-1} - 2\big)\big] + 16 \times 16 \times 2^{2n} \times q \times (8n - 8)$$

$$= 2^{4n} - 3 \times 2^{2n} + 256 \times 2^{2n} \times q(8n - 8) + 2n.$$

Similarly, the time complexity of the preparation for the tensor product representation of quantum color images is also obtained. From the model (4.9), $n + 3$ qubits are needed to construct the quantum image model for a $2^n \times 2^n$ image. To begin with, for the quantum operation of $U_1 = I^{\otimes 3} \otimes H^{\otimes 2n}$, its time complexity is obviously $O(3 + 2n)$.

After this step, the position information for all the pixels is stored in the quantum color image model. It remains to set the *RGB* value for every pixel, where $R_y(\theta_{YX})$ and $R_x(\theta_{YX})$ are the rotations about Bloch sphere's $\hat{y}$ axis and $\hat{x}$ axis by the angle $\theta_{YX}/2$, respectively. Considering the fact that each operation $C^{2n}(R_y(\theta_{YX}^1))$, $C^{2n}(R_x(\theta_{YX}^2))$ and $C^{2n}(R_x(\theta_{YX}^3))$ can be broken down into $3(2^{2n} - 1)$ simple operations and $3(2^{2n} - 2)$ CNOT operations. Of course, it is also necessary to decompose the $C^{2n}(Z)$ gate and the $C^{2n}(S)$ gate to single-quantum and double-quantum gates. So the time complexity of setting the *RGB* value for

Figure 11 An open quantum system model
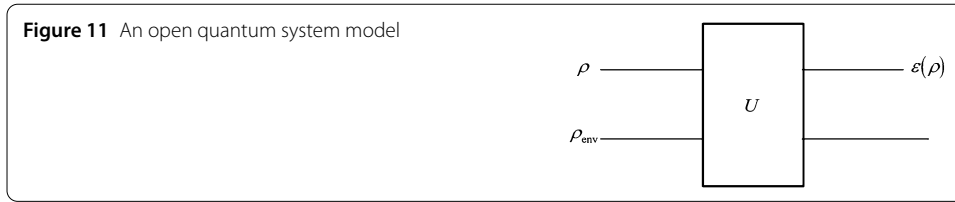
every pixel is no more than $3 \times 16 \times 16 \times 2^{2n} \times q \times (8n - 8)$ with enough ancillary qubits, i.e., $O(qn2^{2n})$.

Therefore, the total number of single-qubit and double-qubit operations used to prepare the tensor product representation of quantum color images is

$$2n + 2^{2n} \times 3\left[\left(2^{2n-1} - 1\right) + \left(2^{2n-1} - 2\right)\right] + 3 \times 16 \times 16 \times 2^{2n} \times q \times (8n - 8)$$

$$= 3 \cdot 2^{4n} - 9 \times 2^{2n} + 768 \times 2^{2n} \times q(8n - 8) + 2n.$$

5 Environments and quantum noise channels

A natural way to describe the dynamics of open quantum systems is to think of them as interactions between the system of interest (here called the principal system) and the environment, which together form a closed quantum system. The dynamics of such a closed quantum system is described by a unitary transformation, and we can think of this unitary transformation as a box. For us, we are not concerned with the internal mechanism of the box, which can be implemented by quantum circuits or some Hamiltonian systems, or even anything else. In other words, suppose we have a system in state ρ, and this state is sent into a box which is coupled to an environment. Then, the final state $\varepsilon(\rho)$ of this system may not be related by a unitary transformation to the initial state ρ.

As illustrated in Fig. 11, we now assume that the input state of the system-environment is a product state $\rho \otimes \rho_{\text{env}}$. After the U transformation of the box, the system no longer interacts with the environment, because we perform a partial trace over the environment to obtain the reduced state of the system alone.

$$\varepsilon(\rho) = \text{tr}_{\text{env}}\left[U(\rho \otimes \rho_{\text{env}})U^\dagger\right] \tag{5.1}$$

This approach is easy to relate to the real world, but it has the disadvantage of being mathematically inconvenient, whereas operator-sum representations for understanding quantum operations, although exactly similar to it, provide a powerful mathematical representation of quantum operations.

If the representation of equation (5.1) is based on the operator on the Hilbert space of the principal system alone, let $|e_k\rangle$ be a set of orthonormal basis of the (finite dimensional) state space of the environment, and then let $\rho_{\text{env}} = |e_0\rangle\langle e_0|$ be the initial state of the environment. Suppose that the environment starts from a pure state, even though the environment is started in a mixed state, we can use it as an intermediate step in the calculation by introducing an additional external system that purifies the environment and does not make any difference to the dynamics experienced by the principal system. Therefore

equation (5.1) can be rewritten as:

$$
\begin{aligned}
\varepsilon(\rho) &= \sum_k \langle e_k | U [\rho \otimes e_0 \rangle \langle e_0 |] U^\dagger | e_k \rangle \\
&= \sum_k E_k \rho E_k^\dagger,
\end{aligned}
\tag{5.2}
$$

where $E_k = \langle e_k | U | e_0 \rangle$ is an operator on the state space of the principal system. The above equation is called the operator-sum representation of ε, and the operator E_k is called the operator element of the quantum operation ε.

We can draw a physical explanation for the operator-sum representation, assuming that after the unitary U transformation, the measurement of the environment is performed on bases $|e_k\rangle$. Applying the principle of implied measurement, it can be seen that such a measurement only affects the state of the environment without changing the state of the principal system. According to this idea, we can deal with noise in the quantum noise channels without affecting the state of the principal system. We regard unnecessary interactions in open quantum systems as noise in quantum information processing, and the processed quantum images as the principal system. In order to build a useful quantum information processing system, we need to understand and control these noise systems without affecting the principal system.

For instance, the amplitude damping channel, which is a quantum operation that describes the energy dissipation of a system to the environment. It is typically an atomic process and can be thought of as the spontaneous emission of a photon into the environment by the decay of an excited state of a two-level atom in the presence of an electromagnetic field. This channel can be described with the map:

$$
|0\rangle_{\text{prin}} |0\rangle_{\text{env}} \to |0\rangle_{\text{prin}} |0\rangle_{\text{env}},
$$

$$
|1\rangle_{\text{prin}} |0\rangle_{\text{env}} \to \sqrt{1-p} |1\rangle_{\text{prin}} |0\rangle_{\text{env}} + \sqrt{p} |0\rangle_{\text{prin}} |1\rangle_{\text{env}}.
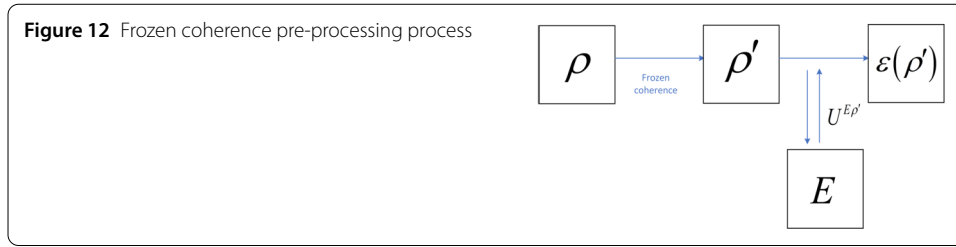$$

When there is no excitation present, the system and the environment remain unaltered, while when an excitation is present in the system, it can either remain itself with probability $(1 - p)$ or decay to $|0\rangle_{\text{prin}} |1\rangle_{\text{env}}$ with probability p, producing an excitation in the environment. So the operator elements of amplitude damping operator ε are

$$
E_0 = \begin{bmatrix} 1 & 0 \\ 0 & \sqrt{1-\gamma} \end{bmatrix} \quad \text{and} \quad E_1 = \begin{bmatrix} 0 & \sqrt{\gamma} \\ 0 & 0 \end{bmatrix},
$$

where $\gamma = \sin^2 \theta$ can be considered as the probability of losing a photon.

If we transmit the quantum gray-scale image in the amplitude damping channel, the quantum image will be in the principal system. After coupling with the environment, the partial trace for the environment can be obtained as follows:

$$
\varepsilon(\rho) = \frac{1}{2^n} \sum_{Y=0}^{2^n-1} \sum_{X=0}^{2^n-1} |Y\rangle \langle X| \otimes \varepsilon\big(\rho_1(\theta_{YX})\big),
\tag{5.3}
$$

Figure 12 Frozen coherence pre-processing process

and specifically speaking,

$$\varepsilon\big(\rho_1(\theta_{YX})\big) = E_0\rho_1(\theta_{YX})E_0^\dagger + E_1\rho_1(\theta_{YX})E_1^\dagger$$

$$= \begin{bmatrix} 1 & 0 \\ 0 & \sqrt{1-\gamma} \end{bmatrix} \begin{bmatrix} \cos^2\frac{\theta}{2} & \cos\frac{\theta}{2}\sin\frac{\theta}{2} \\ \sin\frac{\theta}{2}\cos\frac{\theta}{2} & \sin^2\frac{\theta}{2} \end{bmatrix} \begin{bmatrix} 1 & 0 \\ 0 & \sqrt{1-\gamma} \end{bmatrix}$$

$$+ \begin{bmatrix} 0 & \sqrt{\gamma} \\ 0 & 0 \end{bmatrix} \begin{bmatrix} \cos^2\frac{\theta}{2} & \cos\frac{\theta}{2}\sin\frac{\theta}{2} \\ \sin\frac{\theta}{2}\cos\frac{\theta}{2} & \sin^2\frac{\theta}{2} \end{bmatrix} \begin{bmatrix} 0 & 0 \\ \sqrt{\gamma} & 0 \end{bmatrix}$$

$$= \begin{bmatrix} \cos^2\frac{\theta}{2} + \gamma\sin^2\frac{\theta}{2} & \sqrt{1-\gamma}\cos\frac{\theta}{2}\sin\frac{\theta}{2} \\ \sqrt{1-\gamma}\sin\frac{\theta}{2}\cos\frac{\theta}{2} & (1-\gamma)\sin^2\frac{\theta}{2} \end{bmatrix}$$

$$= \begin{bmatrix} 1 - (1-\gamma)\sin^2\frac{\theta}{2} & \sqrt{1-\gamma}\cos\frac{\theta}{2}\sin\frac{\theta}{2} \\ \sqrt{1-\gamma}\sin\frac{\theta}{2}\cos\frac{\theta}{2} & (1-\gamma)\sin^2\frac{\theta}{2} \end{bmatrix}.$$

If we compare the above result with the original density matrix of the qubit given in (4.6), then we can easily observe that the effect of the coupling with the environment is the introduction of $(1 - \gamma)$ to the density matrix. Meanwhile, the diagonal terms in the density matrix will evolve faster than the off-diagonal terms, which implies that decoherence occurs after the quantum image model is coupled to the noise channel. This coupling will result in the loss of information from the principal system into the environment. Therefore, the model (5.3) provides the foundation for the quantification and protection of coherence in open quantum systems.

In an open quantum system, a quantum image may face the phenomenon of "decoherence" during transmission due to interference from the external environment, resulting in the quantum state become incoherence state. However, by pre-processing the quantum image, we can make its gray scale information satisfy the condition of frozen coherence, which greatly protects the coherence during transmission / process and maintains the clarity of the image at the same time. This process can be depicted as shown in Fig. 12. This performance enhancement in coherence protection will not only enable more secure and reliable quantum communication / process, leading to higher resolution and clearer images, but will also advance the development of some application fields such as quantum cryptography and so on.

The quantum image representation models proposed in the paper are also applicable to various other noise channels, such as bit-flip, bit-phase flip, phase-flip channels, and the phase damping channel. Their action on the quantum image model is described below in terms of a parameter $q \in [0, 1]$ which encodes the strength of the noise. The bit-flip,

bit-phase flip, and phase-flip channels can be represented in operator form by

$$E_0^{F_k} = \sqrt{1 - \frac{q}{2}} I \quad \text{and} \quad E_k^{F_k} = \sqrt{\frac{q}{2}} \sigma_k,$$

with $k = 1, 2$ and 3, respectively, and σ_j being the j-th Pauli matrix. Finally, the phase damping channel can be characterized by

$$E_0 = \begin{bmatrix} 1 & 0 \\ 0 & \sqrt{1 - \gamma} \end{bmatrix} \quad \text{and} \quad E_1 = \begin{bmatrix} 0 & 0 \\ 0 & \sqrt{\gamma} \end{bmatrix}.$$

6 Conclusion

The focus of this paper is to address the problem of quantum image representation encountered in the field of open quantum systems. In the paper, the shortcomings of these existing quantum image models are first identified by analyzing the quantum systems that exist in reality. Since the quantum system inevitably interacts with other quantum systems around it and becomes an open quantum system, the previous image representation methods are only applicable to closed quantum systems. To overcome this problem, we introduce a density matrix to store the gray values of all the pixels in the image instead of the probability amplitude or the information of the qubit sequence. Inspired by incoherent-coherent states, we propose three models for quantum image representation. When encountering the preparation of mixed states, unlike the previous approach of introducing a reference system to make the mixed system a purely entangled state, we deal with the preparation of mixed states through the mapping relation between mixed and pure states on the Bloch sphere, and utilize the rotation operator acting on the Bloch sphere in the preparation process. These models can better capture the coherence and entanglement between pixels in an image, leading to more accurate image representations. However, our proposed model has some limitations, such as the geometrical relations required during the preparation of the MSR-QCI model, which is so complex that the preparation process is relatively difficult. In addition, we investigate the transmission process of quantum images in noisy channels. This is of great significance to the field of quantum communication and image transmission. The results can help us understand how quantum images are affected by noise and provide corresponding error correction and freezing methods. Through these studies, we give a quantum image representation with practical significance in open quantum systems and provide a theoretical basis and practical method for quantum image transmission.

With comparative analysis in our research, we demonstrate the advantages of the new approach over traditional quantum image representation methods, this provides an important background for future related work. Specifically, the use of density matrices representing the quantum images can advance the quantization of quantum images in the coherence domain, enabling the features of coherence changes to be captured in a mathematically rigorous manner. In quantum communication or evolution, we want the transmitted or evolved quantum information to maintain a certain degree of coherence, i.e., not to be distorted by the interference of the external environment that causes the information to be distorted. And frozen coherence helps to obtain a relatively long decoherence time to ensure that the coherence is maintained during gate operation. By studying the frozen

coherence, one can design more stable and reliable quantum communication systems and promote the development of quantum technology in practical applications.

The quantification of coherence generally uses three functions: l_1-norm coherence, relative entropy, and quantum fidelity [38]. Similar to the frozen coherence process that we will discuss in the future, the general conditions for frozen coherence based on quantum fidelity could be explored based on the change of quantum fidelity coherence distance before and after quantum image evolution. These different methods of coherence quantization provide us with a more comprehensive view, allowing us to better understand the properties of quantum images and providing new ideas and methods for future researches.

Abbreviations
QIP, Quantum image processing; PQIR, Problem of quantum image representation; FRQI, Flexible representation of quantum images; NEQR, Novel enhanced quantum representation of digital images; MSR-QCI, Mixed state representation of quantum color images.

Author contributions
Yingying Hu and Dayong Lu wrote the main manuscript text and Qianqian Zhang prepared all the figures. All authors reviewed the manuscript.

Data Availability
No datasets were generated or analysed during the current study.

Code availability
Not applicable.

Declarations

Ethics approval and consent to participate
Not applicable.

Consent for publication
The Author confirms: that the work described has not been published before; that it is not under consideration for publication elsewhere; that its publication has been approved by all co-authors.

Competing interests
The authors declare no competing interests.

Author details
[1]School of Mathematics and Statistics, Henan University, Kaifeng, 475001, China. [2]School of Mathematics and Statistics, Henan University of Science and Technology, Luoyang, 471000, China.

References
1. Nielsen MA, Chuang IL. Quantum computation and quantum information. New York: Cambridge University Press; 2000.
2. Gonalez RC, Woods RE, Eddins SL. Digital image processing. Beijing: Publishing House of Electronics Industry; 2002.
3. Fei Y, Venegas-Andraca SE. Quantum image processing. Singapore: Springer; 2020.
4. Chen GL, Song XH, Venegas-Andraca SE. Qirhsi: novel quantum image representation based on hsi color space model. Quantum Inf Process. 2021;21:5. https://doi.org/10.1007/s11128-021-03337-0.
5. Grigoryan AM, Agaian SS. New look on quantum representation of images: Fourier transform representation. Quantum Inf Process. 2020;19:148. https://doi.org/10.1007/s11128-020-02643-3.
6. Khan RA. An improved flexible representation of quantum images. Quantum Inf Process. 2019;18:201. https://doi.org/10.1007/s11128-019-2306-6.
7. Chen X, Liu ZH, Chen HW, Xu CZ. Qipc: a novel quantum representation model for polar coordinate images. Quantum Inf Process. 2022;21:174. https://doi.org/10.1007/s11128-022-03517-6.
8. Venegas-Andraca SE, Bose S. Storing, processing and retrieving an image using quantum mechanics. In: Proceedings of the SPIE conference on quantum information and computation. 2003. p. 137–47.
9. Venegas-Andraca SE, Ball JL, Burnett K, Bose S. Processing images in entangled quantum systems. Quantum Inf Process. 2010;9:1–11. https://doi.org/10.1007/s11128-009-0123-z.
10. Latorre JI. Image compression and entanglement. 2005. Preprint. arXiv:quant-ph/0510031.

11. Le PQ, Dong F, Hirota K. A flexible representation of quantum images for polynomial preparation, image compression, and processing operations. Quantum Inf Process. 2011;10(1):63–84. https://doi.org/10.1007/s11128-010-0177-y.
12. Zhang Y, Lu K, Gao Y, Wang M. A novel enhanced quantum representation of digital images. Quantum Inf Process. 2013;12:2833–60. https://doi.org/10.1007/s11128-013-0567-z.
13. Isar A, Sandulescu A, Scutaru H, Stefanescu E, Scheid W. Open quantum systems. Int J Mod Phys E. 1994;3(02):635–714. https://doi.org/10.1142/S0218301394000164.
14. Schlosshauer M. Quantum decoherence. Phys Rep. 2019;831:1–57. https://doi.org/10.1016/j.physrep.2019.10.001.
15. Pathak A. Elements of quantum computation and quantum communication. New York: CRC Press; 2013.
16. Gyongyosi L, Imre S. Advances in the quantum Internet. Commun ACM. 2022;65(8):52–63. https://doi.org/10.1145/3524455.
17. Gyongyosi L, Imre S. Scalable distributed gate-model quantum computers. Sci Rep. 2021;11(1):5172. https://doi.org/10.1038/s41598-020-76728-5.
18. Gyongyosi L, Imre S, Nguyen HV. A survey on quantum channel capacities. IEEE Commun Surv Tutor. 2018;20(2):1149–205. https://doi.org/10.1109/COMST.2017.2786748.
19. Baumgratz T, Cramer M, Plenio MB. Quantifying coherence. Phys Rep. 2014;113(14):140401. https://doi.org/10.1103/PhysRevLett.113.140401.
20. Yu XD, Zhang DJ, Xu GF, Tong DM. Alternative framework for quantifying coherence. Phys Rev A. 2016;94(6):060302. https://doi.org/10.1103/PhysRevA.94.060302.
21. Aberg J. Quantifying superposition. 2006. figshare. arXiv:quant-ph/0612146.
22. Jiang N, Wang L. Quantum image scaling using nearest neighbor interpolation. Quantum Inf Process. 2015;14(11):1559–71. https://doi.org/10.1007/s11128-014-0841-8.
23. Zhang R, Xu MY, Lu DY. A generalized floating-point quantum representation of 2-d data and their applications. Quantum Inf Process. 2020;19(11):390.
24. Dong H, Lu DY, Sun XY. Symmetric ternary quantum Fourier transform and its application. Quantum Inf Comput. 2022;22(9–10):733–54. https://doi.org/10.26421/QIC22.9-10-2.
25. Li C, Lu DY, Dong H. Quantum representations and scaling up algorithms of adaptive sampled-data in log-polar coordinates. Entropy. 2021;23(11):1462. https://doi.org/10.3390/e23111462.
26. Yin HT, Lu DY, Zhang R. Quantum windowed Fourier transform and its application to quantum signal processing. Int J Theor Phys. 2021;60(10):3896–918. https://doi.org/10.1007/s10773-021-04933-7.
27. Xu MY, Shang YL. Mfqs: multichannel floating-point quantum representation of digital signals. J Phys Soc Jpn. 2024;93(2):024005. https://doi.org/10.7566/JPSJ.93.024005.
28. Seidel R, Tcholtchev N, Bock S, Becker CK, Hauswirth M. Efficient floating point arithmetic for quantum computers. IEEE Access. 2022;10:72400–15. https://doi.org/10.1109/ACCESS.2022.3188251.
29. Andreadakis F, Anand N, Zanardi P. Scrambling of algebras in open quantum systems. Int J Theor Phys. 2023;107:042217. https://doi.org/10.1103/PhysRevA.107.042217.
30. Kuang R, Perepechaenko M. Quantum encryption with quantum permutation pad in ibmq systems. EPJ Quantum Technol. 2022;9:26. https://doi.org/10.1140/epjqt/s40507-022-00145-y.
31. Abbas A, Sutter D, Zoufal C, Lucchi A, Figalli A, Woerner S. The power of quantum neural networks. Int J Theor Phys. 2021;1:403–9. https://doi.org/10.1038/s43588-021-00084-1.
32. Reh M, Schmitt M, Garttner M. Time-dependent variational principle for open quantum systems with artificial neural networks. Int J Theor Phys. 2021;127(23):230501. https://doi.org/10.1103/PhysRevLett.127.230501.
33. Schumacher B, Nielsen MA. Quantum data processing and error correction. Phys Rev A. 1996;54(4):2629. https://doi.org/10.1103/PhysRevA.54.2629.
34. Chitambar E, Streltsov A, Rana S, Bera MN, Adesso G, Lewenstein M. Assisted distillation of quantum coherence. Phys Rev Lett. 2016;116(7):070402. https://doi.org/10.1103/PhysRevLett.116.070402.
35. Zhao MJ, Ma T, Ma YQ. Coherence evolution in two-qubit system going through amplitude damping channel. Sci China, Phys Mech Astron. 2018;61(020311):1–6. https://doi.org/10.1007/s11433-017-9095-7.
36. Streltsov A, Adesso G, Plenio M. Colloquium: quantum coherence as a resource. Rev Mod Phys. 2017;89(4):041003. https://doi.org/10.1103/RevModPhys.89.041003.
37. Benjamin S. Sending entanglement through noisy quantum channels. Phys Rev A. 1996;54(4):2614. https://doi.org/10.1103/PhysRevA.54.2614.
38. Shao LH, Xi ZJ, Fan H, Li YM. The fidelity and trace norm distances for quantifying coherence. Phys Rev A. 2015;91(4):042120. https://doi.org/10.1103/PhysRevA.91.042120.

Publisher's Note